Fracture Behavior of Thermoplastic Polyolefin/Clay Nanocomposites

S. C. Tjong, Y. H. Ruan

Department of Physics and Materials Science, City University of Hong Kong, Tat Chee Avenue, Kowloon, Hong Kong

Received 12 December 2007; accepted 11 April 2008
DOI 10.1002/app.28560
Published online 10 July 2008 in Wiley InterScience (www.interscience.wiley.com).

ABSTRACT: A thermoplastic polyolefin (TPO) containing 70 wt % styrene–ethylene–butadiene-styrene-*g*-maleic anhydride and 30 wt % polypropylene and its nanocomposites reinforced with 0.3–1.5 wt % organoclay were prepared by melt mixing followed by injection molding. The mechanical and fracture behaviors of the TPO/clay nanocomposites were investigated. The essential work of fracture (EWF) approach was used to evaluate the tensile fracture behavior of the nanocomposites toughened with elastomer. Tensile tests showed that the stiffness and tensile strength of TPO was enhanced by the addition of low loading levels of organically modified montmorillonite. EWF measurements revealed that the fracture toughness of the TPO/clay nanocomposites increased with increasing clay content. The organoclay toughened the TPO matrix of the nanocomposites effectively. © 2008 Wiley Periodicals, Inc. J Appl Polym Sci 110: 864–871, 2008

Key words: clay; elastomers; nanocomposites; toughness

INTRODUCTION

Thermoplastic elastomer (TPE) blends are polymeric materials consisting of thermoplastics and elastomers. They combine the good processability and plastic deformability of thermoplastics with the large elastic response of elastomers. The most commonly used elastomers include ethylene–propylene rubber (EPR), ethylene–propylene–diene terpolymer rubber (EPDM), styrene–ethylene–butadiene–styrene (SEBS), and polyethylene octane elastomer. A typical example of TPE is thermoplastic polyolefin (TPO), which generally consists of about 70 wt % isotactic polypropylene (PP) and 30 wt % EPR. In this blend, PP comprises the major phase and acts as the matrix of TPO. The dispersed elastomer phase serves to improve the toughness and impact strength of PP. TPO blends are widely used in many industrial applications because of their excellent weather resistance, low density, and low cost. However, their mechanical strength and stiffness are relatively low compared to those of thermoplastics. In this regard, TPO blends are mostly compounded with inorganic fillers such as talc to improve their mechanical strength. Such filler-reinforced TPO materials are widely used to produce automotive parts. However, these microcomposites require the use of large amounts of fillers, typically in the range 20–30 wt %. This leads to poor processability and extensive wear of the compounding facilities.

In the past decade, layered silicate clays such as montmorillonite have attracted considerable attention for the strengthening of polymers because of their unique properties, such as large aspect ratio, high surface area, and low cost. The addition of low loading levels of silicate clays to polymers markedly improves their tensile strength, stiffness, and heat resistance. Lower clay loadings facilitate processing and reduce component weight. The high aspect ratio and large surface area of the clay nanolayers offer high reinforcing efficiency for the polymers. Thus, silicate clays are also effective nanofillers for reinforcing TPO. TPO-based nanocomposites have found applications as a step assist for the 2002 General Motors Safari and Chevrolet Astro vans.[1,2]

The morphology and mechanical behavior of TPE reinforced with silicate clays have been studied by many research groups.[3–6] On the basis of transmission electron microscopy and atomic force microscopy observations, Paul et al.[5] reported that the size of elastomer particles and the aspect ratio of the clay particles tended to decrease with increasing clay content. Furthermore, the mechanical properties of TPO-based nanocomposites depend greatly on the clay and elastomer contents. Supertough nanocomposites with significantly high impact strengths can be achieved by the addition of 30–40% rubber and 2–7 wt % montmorillonite to PP. In other words, the clay nanoplatelets strengthen, stiffen, and toughen the TPO matrix. However, these studies have mainly

Correspondence to: S. C. Tjong (aptjong@cityu.edu.hk).

focused on the morphology and mechanical behavior of TPO/clay nanocomposites with a PP matrix. Little information is available TPO/clay nanocomposites with elastomer matrices. Very recently, Mishra et al.[7] prepared TPO/clay nanocomposites in which the TPO contained 25 wt % PP and 75 wt % EPDM. They reported that the nanocomposites exhibited remarkable improvements in the tensile and storage moduli over their pristine TPO blend. Austin and Kontopoulou[8] also incorporated organoclay into a rubber-rich TPO [30% PP and 70% EPR-*g*-maleic anhydride (MA)] to improve its stiffness and thermal stability. It is widely known that EPDM is a typical unsaturated polyolefin rubber that is widely used in the fabrication of automotive tire sidewalls, wires, cables, footwear, and sporting goods. To improve the mechanical strength, hardness, and abrasion resistance of this soft rubber, carbon black microparticles are often added.[9,10] Recently, some researchers have used organoclay to reinforce EPDM and other types of rubbers, as low loading levels of clays are needed to achieve the desired properties.[11,12] Organoclay additions are considered to also be beneficial for the enhancement of the mechanical properties of rubber-rich TPO blends. Their appear to be no studies thus far on the toughening mechanism of TPO/clay nanocomposites having a maleated SEBS matrix. In this study, we mainly aimed to investigate the effects of organoclay additions on the fracture toughness of such nanocomposites prepared by melt compounding. The fracture toughness of such nanocomposites was evaluated with the essential work of fracture (EWF) method under the tensile mode.

EXPERIMENTAL

Materials

The organically modified montmorillonite (OMMT) used was Cloisite 30B [(bis(2-hydroxyethyl) methyl tallow ammonium montmorillonite)], which was supplied from Southern Clay Products. PP (Profax 6331), with a melt flow index of 12 g/10 min, and poly(styrene–ethylene–butylene–styrene) grafted with 1.84 wt % MA (SEBS-*g*-MA; Kraton FG 1901X) were purchased from Himont Co. and Shell Co., respectively. All of the polymeric materials and OMMT were dried at 80°C for 24 h before melt processing.

Nanocomposite preparation

A two-step compounding process was used to prepare the TPO nanocomposites. This involved an initial melt mixing of OMMT with PP followed by the melt compounding of PP/OMMT products with SEBS-*g*-MA in a twin-screw Brabender extruder. The blending temperature was set at 200°C. The ratio of PP to SEBS was fixed at 30 : 70 by weight. The clay loadings varied from 0.3 to 1.5 wt %. The TPO nanocomposites reinforced with 0.3, 0.6, 1.2, and 1.5 wt % OMMT are designated as 1TPO, 2TPO, 3TPO, and 4TPO, respectively. The extrudates were then pelletized and dried again before injection molding. Subsequently, the TPO pellets were directly injection-molded into plaques.

X-ray diffraction (XRD) measurement

XRD measurements were performed with a diffractometer (Simens D500) equipped with Ni-filtered Cu Kα radiation with a wavelength of 0.154 nm. The diffractometer was operated at 30 kV. The scanning rates were 1°/min over a 2θ range of 1–10°.

Fourier transform infrared (FTIR) spectroscopy

The FTIR spectra were collected with a FTIR spectrometer (16PC FTIR, PerkinElmer) in transmission mode. The samples were scanned within the range 4000–400 cm^{-1} with a resolution of 4 cm^{-1}. To prepare the clay specimen, KBr was introduced into pure clay; this mixture was then pressed into a disc 1–2 mm thick. The TPO nanocomposite and SEBS-*g*-MA specimens were directly hot-pressed into films about 40–60 μm thick.

TEM

TEM specimens were cut from the injection-molded plaque with a Reichert Ultracut microtome. The films were placed onto the Cu grids and then placed into the specimen chamber of a transmission electron microscope (Philips CM-20).

Tensile behavior

Tensile tests were carried out with an Instron 5567 instrument at room temperature according to ASTM D 638. Young's modulus was measured with an extensometer at a crosshead speed of 10 mm/min. The tensile strength was determined at a crosshead speed of 100 mm/min. Five specimens of each material were used for the tensile measurements, and the average values were reported.

Fracture toughness characterization

Double-edge notched tension (DENT) specimens with dimensions of 100 $\times$ 38 $\times$ 3.2 mm^3 were used (Fig. 1). They were cut from the injection-molded plaques, in which the longitudinal direction of the specimens was parallel to the melt flow direction.

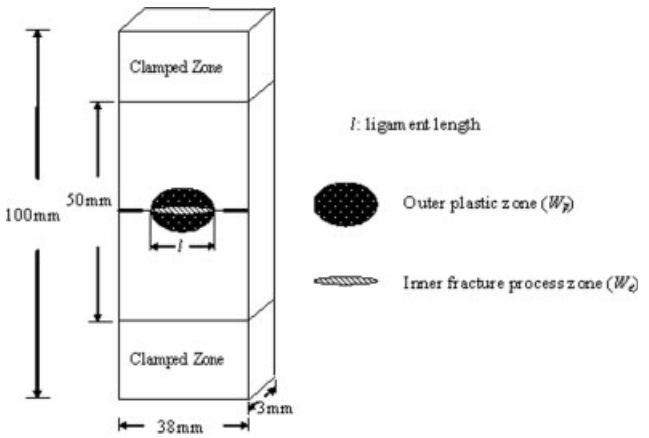

Figure 1 Geometry of the DENT specimen.

We made the notches first by forming saw cut slots and then by sharpening them with a fresh razor blade. The exact ligament length (l) was measured with a traveling microscope (Tropcon profile projector). The gauge length of the sample was 50 mm. The DENT samples were loaded in an Instron tensile tester (model 5567) with a crosshead speed of 1 mm/min. Load versus displacement plots for the specimens were recorded.

RESULTS AND DISCUSSION

Structure

The XRD patterns of the OMMT and TPO nanocomposites are shown in Figure 2. The pristine organoclay showed a distinct diffracting peak (d_{001}) at $2\theta = 4.9^\circ$, which corresponded to an interlayer spacing of 1.79 nm. With the addition of 0.3–0.6 wt % OMMT to TPO, this diffracting peak disappeared. Generally, the disappearance of diffracting peaks would indicate a destroyed structure, exfoliation, full disordering (meso), or limited sensitivity. In this study, the absence of diffracting peaks indicated the formation of exfoliated nanocomposites. In the case of intercalated composites, polymer chains are readily inserted into the clay galleries during compounding. The clay platelets are still organized into an ordered structure despite swelling of the galleries. The formation of either intercalated or exfoliated nanocomposites can be confirmed by TEM. Figure 3(a,b) shows representative TEM micrographs of the 4TPO nanocomposite. These micrographs reveal the formation of an intercalated structure. The insertion of polymer chains into the clay galleries increased the clay spacing compared to the pristine OMMT. The absence of diffraction peaks in the XRD patterns should not be used as sole evidence for the formation of an exfoliated structure. This is because factors such as clay dilution and peak broadening can yield false results that show that exfoliation has occurred. Other factors, such as the preferred orientation

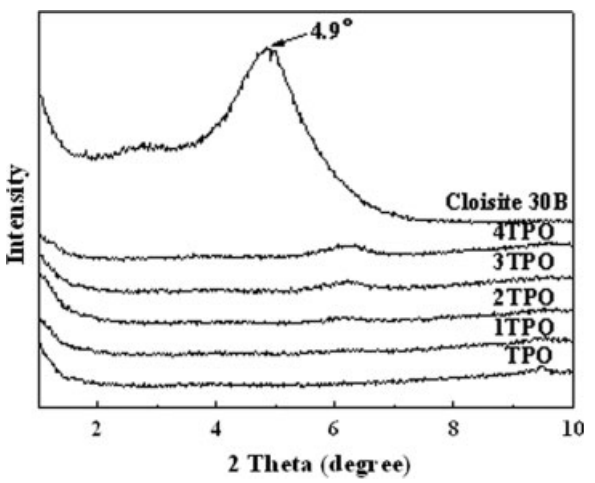

Figure 2 XRD patterns of OMMT, TPO, and their nanocomposites.

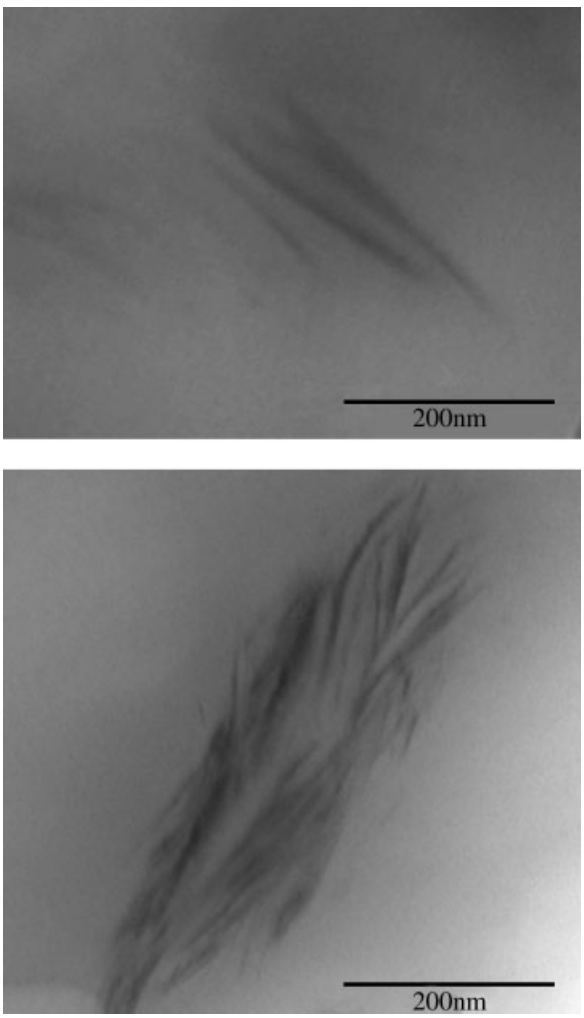

Figure 3 (a) Low and (b) higher magnification TEM micrographs of the 4TPO nanocomposite showing the formation of an intercalated structure.

TABLE I
Properties of TPO and Its Nanocomposites

Specimen	Young's modulus (MPa)	Tensile strength (MPa)
TPO	118.56	8.95
1TPO	118.97	9.00
2TPO	122.36	9.02
3TPO	140.18	9.20
4TPO	142.70	9.32

effect, can produce false conclusions that exfoliation has not occurred.[13] From these, it is apparent that the XRD pattern alone does not accurately predict the dispersion of silicate platelets in polymeric matrix. In this regard, TEM can provide useful information and conclusive remarks concerning the morphology, structure, and spatial distribution of dispersed clay platelets in the polymer matrix.[14]

Tensile behavior

The mechanical properties of the investigated TPO nanocomposites are listed in Table I. The results show that the OMMT additions improved the stiffness and mechanical strength of TPO, as expected. There was about a 20% enhancement in the Young's modulus and a 16% increase in the tensile strength with the addition of 1.5 wt % OMMT. The increases in stiffness and strength were attributed to the reinforcing effect of OMMT. This arose from the interaction between the nanoclay platelets and the polymer matrix. In other words, the hydroxyl group of Cloisite 30B interacted with the MA group of SEBS-*g*-MA during melt compounding. Moreover, the restriction on polymer chain rearrangement and mobility exerted by the silicate platelets also contributed to the enhancement of the tensile strength and stiffness.

Figure 4(a) shows the FTIR spectrum of pristine Cloisite 30B. Cloisite 30B is polar organoclay with the organic modifier methyl tallow bis-2-hydroxyethyl ammonium (MT2EtOH) and has the formula:

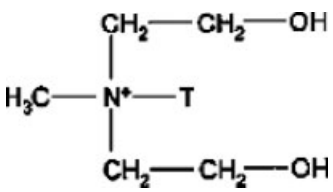

This spectrum displays a sharp band at 3600 cm^{-1} associated with the O—H stretching vibration.[15,16] Figure 4(b) shows the FTIR spectra of the TPO, 1TPO, 2TPO, 3TPO, and 4TPO specimens. For the purpose of comparison, the FTIR spectrum of pure SEBS-*g*-MA is also shown in this figure. The asymmetric and symmetric carbonyl stretching vibration of the free anhydride of all specimens was observed at 1786 and 1866 cm^{-1}, respectively.[17–20] Also, the signal at 1712 cm^{-1} corresponding to carbonyl stretching of free carboxyls was due to the partial hydrolysis of MA rings during the film preparation process for FTIR examination.[19–21] With increasing clay loading, the signal at about 1744 cm^{-1} became obvious because of the hydrogen-bonded carbonyl stretching[22] that resulted from the hydrogen bonding between the carbonyl groups in MA and the hydroxyl groups in the MT2EtOH of Cloisite 30B. Hydrogen bonding between the polymer and Cloisite 30B has been reported by many researchers.[23–27] In general, it was difficult to resolve the complicated FTIR spectrum, not only because of the overlap of the aromatic overtone signals of SEBS (e.g., at about 1704, 1742, 1790, and 1879 cm^{-1})[19] but also because of the very small amount of MT2EtOH in the TPO nanocomposites,[22] that is, the amount of MT2EtOH in Cloisite 30B was 32 wt % and about 0.48 wt % in the 4TPO nanocomposites.

Fracture toughness

In recent years, the EWF concept has been increasingly used to evaluate the fracture toughness of ductile polymers and tough composites. This approach

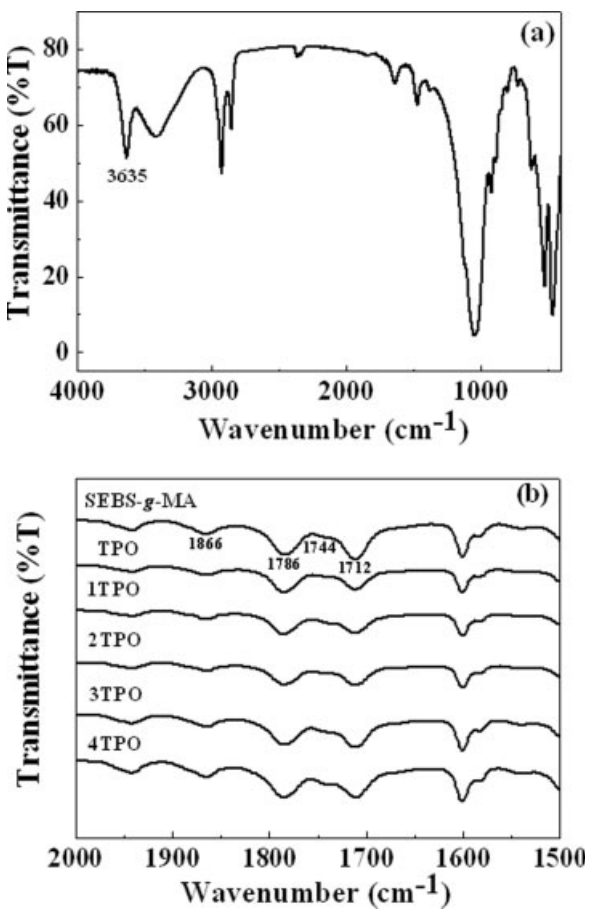

Figure 4 FTIR spectra of the (a) Cloisite 30B and (b) TPO, 1TPO, 2TPO, 3TPO, and 4TPO and SEBS-*g*-MA specimens.

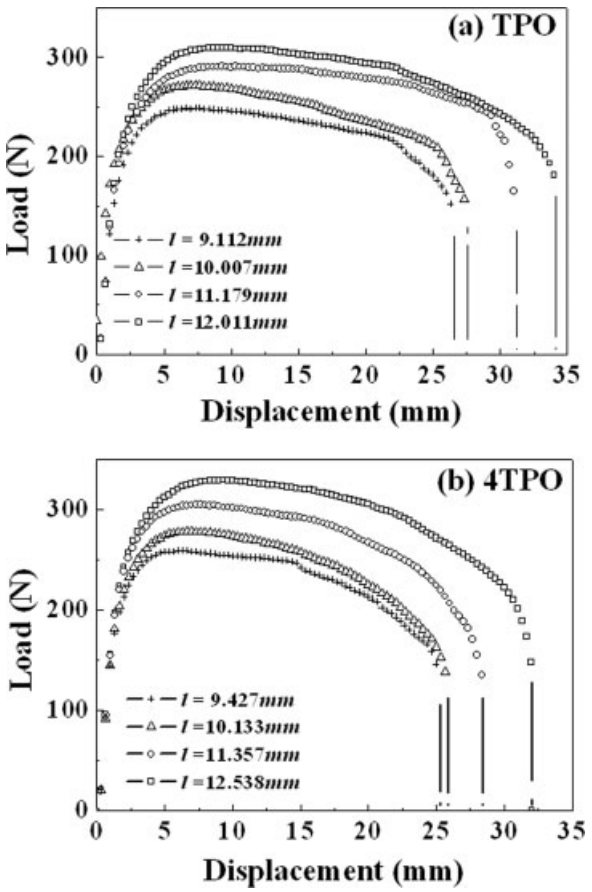

Figure 5 Load-displacement curves for the TPO blend and 4TPO nanocomposite with various l values.

is also very effective for determining the fracture toughness of polymer/clay nanocomposites.[28–38] In a quasistatic tensile test, the total fracture work (W_f) can be divided into two components: one corresponding to the essential work required to fracture the polymer in its process zone (W_e) and another corresponding to the nonessential plastic work (W_p) corresponding to the energy consumed by various deformation mechanisms in the plastic zone. W_f can be expressed as follows:[39–41]

$$W_f = W_e + W_p \tag{1}$$

$$W_f = w_e l t + \beta w_p l^2 t \tag{2}$$

$$w_f = \frac{W_f}{lt} = w_e + \beta w_p l \tag{3}$$

where w_f is the specific total fracture work; w_e and w_p are the specific essential fracture work and specific plastic work, respectively; l is the ligament length; t is the sample thickness; and β is a shape factor of the plastic zone. Apparently, the EWF concept is a simple method that consists of testing specimens with different l values, recording the area under the load displacement curve (W_f), plotting the w_f versus l diagram, and evaluating the best fit regression line. The slope of the w_f versus l linear plot yields w_p, and the intercept produces w_e. The specimen must be fully yielded before crack initiation, which can be easily evaluated from the slow testing of the double-edge notched tensile specimen.

Typical load-displacement curves for the TPO blend and 4TPO nanocomposite with different l values are shown in Figure 5(a,b). It is apparent that the load-displacement curves for different l values were geometric similar to each other. This similarity is a crucial criterion for the suitability of the EWF approach for fracture characterization.[28] Moreover, both the TPO and 4TPO specimens underwent extensive yielding before crack extension. Figure 6(a–e) shows the plots of w_f versus l for TPO and its nanocomposites. These plots revealed that all of the specimens displayed excellent linearity with a high correlation coefficient and minimal scatter in the specific total work. Furthermore, the slope of the linear regression plots tended to decrease with increasing clay content. The results of the tensile EWF measurements for all of the investigated specimens are summarized in Table II. The w_e values of the TPO nanocomposites tended to increase with increasing OMMT content. This implies that the OMMT platelets toughened the TPO matrix effectively. Figure 7(a,b) shows low-magnification SEM fractographs of the TPO and 4TPO specimens after the EWF test. Their corresponding high magnification views are shown in Figure 7(c,d). Wavy shear banding was observed on the fracture surface for TPO, but it was more apparent for the 4TPO nanocomposite. This indicates that the TPO matrix underwent a large-scale deformation during tensile loading. This absorbed considerable energy and led to the highest w_e value or fracture toughness. From the tensile and EWF measurements, we concluded that OMMT was effective in toughening the TPO/clay nanocomposites. In general, the notches of EWF test specimens produce high local stresses (triaxial for plane–strain and biaxial for plane–stress specimens) ahead of the crack tip. However, cavitation of the elastomer and craze initiation tend to relieve such local stress states. Extensive elastomer cavitation and massive crazing can induce shear yielding of the matrix during deformation, as shown in Figure 7(a–d). Crazing and shear yielding involve the high mobility of chain segments during plastic deformation, which thereby contribute to an improvement in fracture toughness.

It is well recognized that the addition of spherical nanoparticles to thermoplastics enhances their toughness considerably. The debonding of such nanoparticles from the polymer matrix and their subsequent cavitation at the constraint yield stress

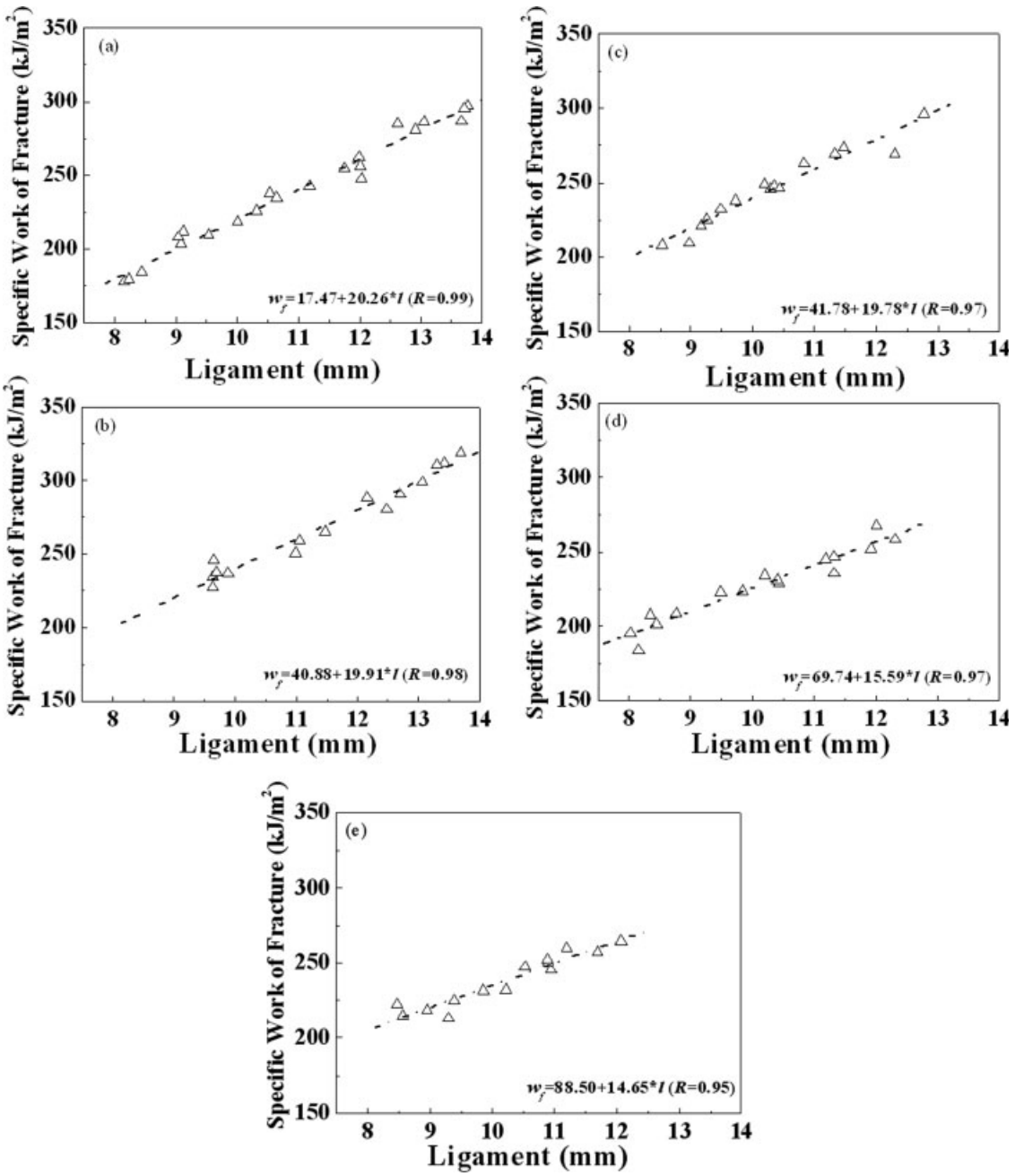

Figure 6 Specific fracture work versus l for the (a) TPO, (b) 1TPO, (c) 2TPO, (d) 3TPO, and (e) 4TPO specimens.

are responsible for improving the toughness of nanocomposites. This effect generally produces multiple crazelike bands with dilatation.[42,43] However, the addition of organoclays to thermoplastics impairs their fracture toughness significantly. It is assumed that the delamination or debonding of stiffer nanoclays from thermoplastics with higher aspect ratios is more difficult when compared to that of spherical particles.[44] In this study, the hydroxyl group of the organoclay (Cloisite 30B) could interact

TABLE II
Specific EWF (w_e) and βw_p for the Specimens Investigated

Specimen	w_e (kJ/m^2)	βw_p (MJ/m^3)	R
TPO	17.47	20.26	0.9884
1TPO	40.88	19.91	0.9819
2TPO	41.78	19.78	0.9700
3TPO	69.74	15.59	0.9659
4TPO	88.50	14.65	0.9510

R = correlation coefficient.

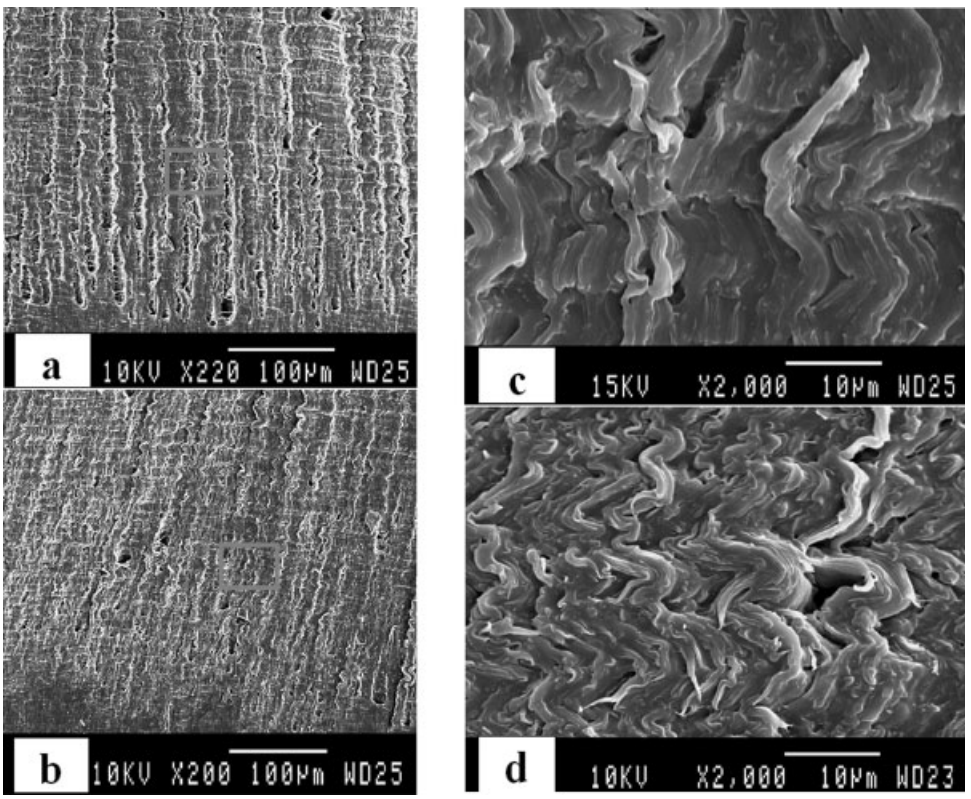

Figure 7 Low-magnification SEM fractographs of the (a) TPO and (b) 4TPO specimens after EWF measurements. (c,d) High-magnification SEM micrographs of areas marked by the square symbol in parts (a) and (b).

with the MA group of SEBS-*g*-MA during melt compounding. This led to the formation of strong bonding between the clay and elastomeric matrix. Therefore, debonding of the nanoclay platelets from ductile SEBS became difficult. The toughness of the nanocomposites was mainly derived from the energy dissipated in the debonding of the clays from SEBS and from the shear yielding of the TPO matrix during tensile deformation.

CONCLUSIONS

TPO/clay nanocomposites reinforced with 0.3–1.5 wt % organoclay were prepared by melt mixing followed by injection molding. The mechanical and fracture behaviors of the TPO/clay nanocomposites were investigated. XRD measurements revealed the absence of a basal diffracting peak of OMMT in the TPO/clay nanocomposites, which implied the destruction of the ordered clay structure and the formation of an intercalated/exfoliated structure. TEM observation showed the formation of an intercalated structure in the nanocomposites. Tensile tests showed that the stiffness and tensile strength of the TPO was enhanced by the addition of low loading levels of OMMT. EWF measurements revealed that the fracture toughness of the TPO/clay nanocomposites increased with increasing clay content. The organoclay was toughened the TPO matrix of the nanocomposites effectively.

References

1. http://www.basell.com.
2. Plast Additives Compd 2001, 3, 8.
3. Lee, K. Y.; Goettler, L. A. Polym Eng Sci 2004, 44, 1103.
4. Mehta, S.; Mirabella, F. M.; Rufener, K.; Bafna, A. J Appl Polym Sci 2004, 92, 928.
5. Lee, H. S.; Fasulo, P. D.; Rodgers, W. R.; Paul, D. R. Polymer 2005, 26, 11673.
6. Kim, D. H.; Fasulo, P. D.; Rodgers, W. R.; Paul, D. R. Polymer 2007, 48, 5960.
7. Mishra, J. K.; Hwang, K. J.; Ha, C. S. Polymer 2005, 46, 1995.
8. Austin, J. R.; Kontopoulou, M. Polym Eng Sci 2006, 46, 1491.
9. Luthern, J. Polymer 1993, 34, 4241.
10. Kurian, T.; De, P. P.; Khastgir, D.; Tripathy, D. K.; De, S. K.; Peiffer, D. G. Polymer 1995, 36, 3875.
11. Zheng, H.; Zhang, Y.; Peng, Z.; Zhang, Y. Polym Test 2004, 23, 217.
12. Lu, Y. L.; Li, Z.; Yu, Z. Z.; Tian, M.; Zhang, L. Q.; Mai, Y. M. Compos Sci Technol 2007, 67, 2903.
13. Eckel, D. F.; Balogh, M. P.; Fasulo, P. D.; Rodgers, W. R. J Appl Polym Sci 2004, 93, 1110.
14. Morgan, A. B.; Gilman, J. W. J Appl Polym Sci 2003, 87, 1329.
15. Mohan, J. Organic Spectroscopy, 2nd ed.; Alpha Science International, Harrow, Ltd.: Middlesex, UK, 2002; p 86.
16. Russell, J. D.; Farmer, V. C. Clay Miner Bull 1964, 5, 443.
17. Bellamy, L. J. The Infrared Spectra of Complex Molecules; Chapman & Hall: London, 1980; Vols. I and II.
18. Colthup, N.; Daly, L.; Wiberley, S. Introduction to Infrared and Raman Spectroscopy; Academic: New York, 1975.

19. Filippi, S.; Yordanov, H.; Minkova, L.; Polacco, G.; Talarico, M. Macromol Mater Eng 2004, 289, 512.
20. Abbate, M.; Lionello, V. Di; Martuscelli, E.; Musto, P.; Ragosta, G.; Scarinzi, G. Polymer 1992, 33, 2940.
21. Kwee, T.; Mauritz, K. A.; Beyer, F. L. Polymer 2005, 46, 3871.
22. Lee, K. M.; Han, C. D. Polymer 2003, 44, 4573.
23. Pattanayak, A.; Jana, S. C. Polymer 2005, 46, 3275.
24. Pattanayak, A.; Jana, S. C. Polymer 2005, 46, 3394.
25. Pattanayak, A.; Jana, S. C. Polymer 2005, 46, 5183.
26. Finnigan, B.; Martin, D. J.; Halley, P.; Truss, R.; Campbell, K. Polymer 2004, 45, 2249.
27. Dan, C. H.; Lee, M. H.; Kim, Y. D.; Min, B. H.; Kim, J. H. Polymer 2006, 47, 6718.
28. Mai, Y. W.; Powell, P. J Polym Sci Part B: Polym Phys 1991, 29, 785.
29. Hashemi, S. Polym Eng Sci 1997, 37, 912.
30. Mouzakis, D. E.; Gahleitner, M.; Karger-Kocsis, J. J Appl Polym Sci 1998, 70, 873.
31. Maspoch, M. L.; Ferrer, D.; Gordillo, A.; Santana, O.; Martinez, A. B. J Appl Polym Sci 1999, 73, 177.
32. Casellas, J. J.; Frontini, P. M.; Carella, J. M. J Appl Polym Sci 1999, 74, 781.
33. Tjong, S. C.; Xu, S. A.; Li, R. K.; Mai, Y. W. Compos Sci Technol 2002, 62, 831.
34. Tjong, S. C.; Xu, S. A.; Li, R. K.; Mai, Y. W. Compos Sci Technol 2002, 62, 2017.
35. Bureau, M. N.; Perrin-Sarazin, F.; Ton-That, M. T. Polym Eng Sci 2004, 44, 1142.
36. Avlar, S.; Qiao, Y. Compos A 2005, 36, 624.
37. Tjong, S. C.; Bao, S. P.; Liang, G. D. J Polym Sci Part B: Polym Phys 2005, 43, 3112.
38. Tjong, S. C.; Bao, S. P. Compos Sci Technol 2007, 67, 314.
39. Broberg, K. B. J Mech Phys Solids 1975, 23, 215.
40. Mai, Y. W.; Cotterell, B. Eng Fract Mech 1985, 21, 123.
41. Mai, Y. W.; Cotterell, B. Int J Fract 1986, 32, 105.
42. Tjong, S. C. Mater Sci Eng R 2006, 53, 73.
43. Zhang, Q. X.; Yua, Z. Z.; Xie, X. L.; Mai, Y. W. Polymer 2004, 45, 5985.
44. Cotterell, B.; Chia, J. Y.; Hbaieb, K. Eng Fract Mech 2007, 74, 1054.